PROCEEDINGS OF THE INTERNATIONAL CONFERENCE
NANOMATERIALS: APPLICATIONS AND PROPERTIES
Vol. **3** No 1, 01NTF22(4pp) (2014)

Structure and Properties NbN and Nb-Si-N Deposited by Magnetron Sputtering

V.I. Ivashchenko[1], P.L. Scrynskyy[1], O.S. Lytvyn[2], V.M. Rogoz[3,*], O.V. Sobol[4], A.P. Kuzmenko[5]

[1] *Institute for Problems of Material Science, NASU, 3, Krzhyzhanovsky Str., 03680 Kiev - 142, Ukraine*
[2] *Institute of Semiconductor Physics, NASU, 41, Nauky Pr., 03028 Kyiv, Ukraine*
[3] *Sumy State University, 2, Rimsky-Korsakov Str., 40000 Sumy, Ukraine*
[4] *National Technical University "KPI", 21, Frunze Str. , 61002 Kharkov, Ukraine*
[5] *Kursk State Technical University, Center for collective use "High Tech", 94, October 50 Str., 305040 Kursk, Russia*

(Received 29 July 2014; published online 29 August 2014)

NbN and Nb-Si-N films were deposited by magnetron sputtering the Nb and Si targets on silicon wafers at various bias voltage, U_s. The films were investigated by an atomic force microscope (AFM), X-ray diffraction (XRD), X-ray photoelectron spectroscopy (XPS) and nanoindentation. The deposited films were annealed to establish their thermal stability. The NbN films were nanostructured, and the Nb-Si-N films had a nanocomposite structure, and represented an aggregation of δ-NbN_x nanocrystallites embedded into the amorphous Si_3N_4 tissue (nc-δ-NbN_x/ a-Si_3N_4).

Keywords: AFM, XRD, NbN, Nb-Si-N, XPS.

PACS numbers: 61.05.C –, 61.05.cp, 68.37.Ps, 61.05.js

1. INTRODUCTION

Nanostructured films are widely used for surface hardening of cutting tools due to high hardness, good corrosion stability and low friction coefficient [1-7]. Among these films, NbN-based films are of increasing interest. The hardness of such binary NbN nitride films is much more high than the bulk material (HV = 14 GPa) and higher than other binary nitride films (TiN, ZrN, VN). The hardness of the NbN films deposited by different arc deposition systems reaches 34-49 GPa [8]. The NbN films were also prepared by using magnetron sputtering (MS) [9], ion beam assisted deposition [10], pulsed laser deposition [11]. An increase in hardness was reached by the formation of the nanocomposite or nanolayered structures of the films based on niobium nitride. Silicon nitrides are known for their high temperature stability, low friction coefficient and high oxidation resistance. Hence, one can expect that that Nb-Si-N nanocomposite and multilayers will combine the properties of the constituent materials and will have improved properties as compared to NbN. In further, we will put an accent on the films prepared with magnetron sputtering. We reviewed the recent investigations on NbN and Nb-Si-N films deposited by magnetron sputtering.

We see from this brief review that, despite the previous investigations of the NbN and Nb-Si-N films, the comparative study of these two kinds of films prepared at the same deposition parameters was not yet carried out. Also, so far, the effect of the bias voltage supplied to the substrate (U_s) on film properties was not analyzed. Besides, we note that, up to date, any theoretical investigations of the NbN/SiN_x nanostructures at the atomic level were not carried out.

In this work we aimed to fill these gaps in the investigations of NbN and Nb-Si-N films. These films were deposited on silicon wafers at various Us. The films were then investigated by: an atomic force microscope (AFM), X-ray diffraction (XRD), X-ray photoelectron spectroscopy (XPS), nanoindentaion and microindentation. The deposited nanocomposite films were annealed to establish their thermal stability. The NbN(001)/Si_3N_4 heterostructures were calculated at various temperature using first-principles molecular dynamics simulations to interpret the experimental results on the Nb-Si-N films.

2. EXPERIMENTAL AND COMPUTATIONAL DETAILS

The NbN-based films were deposited on the mirror-polished Si (100) wafer by DC magnetron sputtering the Nb (99.9 %, Ø72×4 mm) and Si (99.999 %, Ø72×4 mm) targets in an argon-nitrogen atmosphere at the following deposition parameters: substrate temperature T_S= 3500°C; substrate bias U_s = 0 V, -20 V -40 V, -70 V; flow rate (F) F_{Ar} = 40 sccm; F_{N2} = 13 sccm; working pressure P_C = 0.17 Pa. The current applied to the Nb target was 150, 200, 250 and 300 mA, which corresponded to a discharge power density P_{Nb} = 17.1 W/cm^2, respectively. The current on the Si target was 100 mA (P_{Si} = 5.3 W/cm^2). The base pressure of the vacuum chamber was better than 10^{-4} Pa. The distance between the targets and the substrate holder was 8 cm. The dihedral angle between the target planes was ~ 450. The substrates were cleaned ultrasonically before they were put into the vacuum chamber. Also, before deposition, the substrates were etched in the vacuum chamber in hydrogen plasma during 5 min. The film deposited at P_{Nb} = 14.3 W/cm^2 was annealed in a vacuum (0.001 Pa) during 2 ours at 600, 800 and 1000°C.

The crystal structure of the films was determined by X-ray diffraction (XRD, diffractometer DRON-3M) using CuK_α radiation. The crystallite size in films was evaluated from the broadening of peaks in X-ray diffraction spectra using Scherrer formula. The chemical

*v.rogoz2009@gmail.com

 © 2014 Sumy State University

bonding status of films was observed by X-ray photoelectron spectroscopy (XPS, EC 2401, USSR) using MgK_α radiation (E=1253.6 eV). The Au 4f7/2 and Cu 2p3/2 peaks with binding energy at 84.0 ± 0.05 eV and 932.66±0.05 eV, respectively, were used as a reference. Surface morphology was analyzed by atomic force microscope (AFM) NanoScope IIIa Dimension 3000 (Digital Instruments, USA). The hardness and elastic modulus of films were determined from indentation by Nanoindenter-G200 instrument equipped with a Berkovich pyramidal tip under load in the range of 9 - 13 mN. This range of loads was chosen in order to obtain prominent plastic deformation of film while avoiding the influence of substrate material. The nanohardness (H) and elastic modulus (E) data was obtained from the load-displacement curves using Oliver and Pharr method. The Knoop hardness (HK) was estimated by a Microhardness Tester Micromet 2103 BUEHLER LTD at loading of 100 mN.

3. RESULTS AND DISCUSSION

Figure 1 shows the AFM surface topography of the NbN and Nb-Si-N films deposited at various U_s. One can see that the film surface roughness increases with U_s. Also, the surface roughness in Nb-Si-N films is smaller than in NbN films, which can be due to the availability the amorphous SiN_x tissue in Nb-Si-N films (see below). It follows that a decrease in the bias voltage Us and an introduction of silicon promote the reduction of surface roughness.

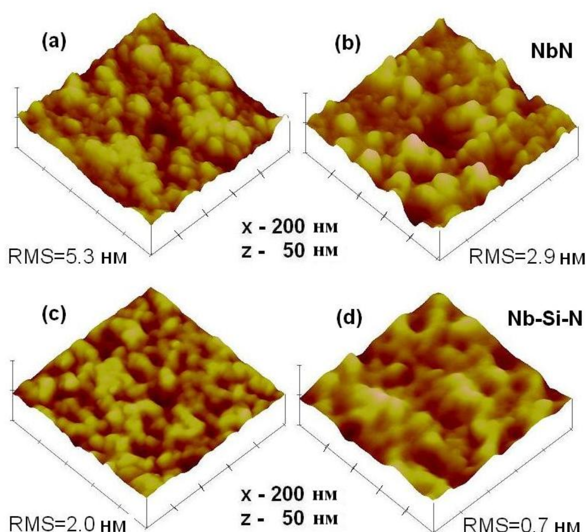

Fig. 1 – AFM images of: the NbN films deposited at U_s = 0 V (RMS = 5.3 nm) (a) and U_s = -70 V (RMS = 2.9 nm) (b); Nb-Si-N films deposited at U_s = 0 V (RMS = 2.0 nm) (c) и U_s = -70 V (RMS = 0.7 nm) (d)

The XRD spectra of the deposited NbN and Nb-Si-N films are shown in Fig. 2 and Fig. 3. The peak A at 35.1 - 35.40 and the peak B at 41.1 - 41.40 can be assigned to the δ-NbN_x(111) and δ-NbN_x(200) reflections, respectively. The grain size estimated from the Scherrer formula was in the ranges 4.1 − 8.7 nm and 18.1 - 19.8 nm for the NbN and Nb-Si-N films, respectively. It follows that an introduction of Si leads to an increase of the NbN grains.

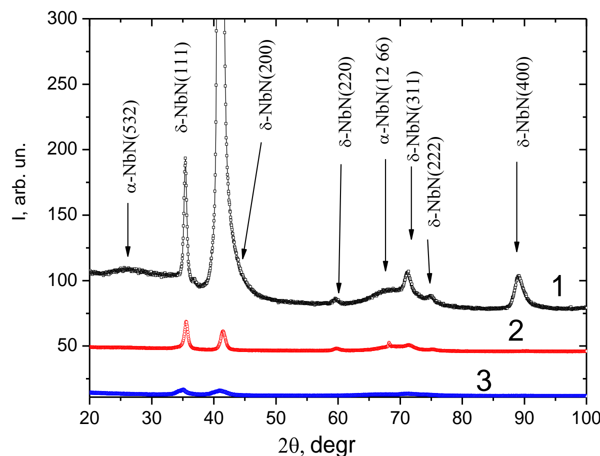

Fig. 2 – XRD spectra of NbN films at 1. U_s = 0 V, 2. U_s = − 40 V, 3. U_s= - 70 V

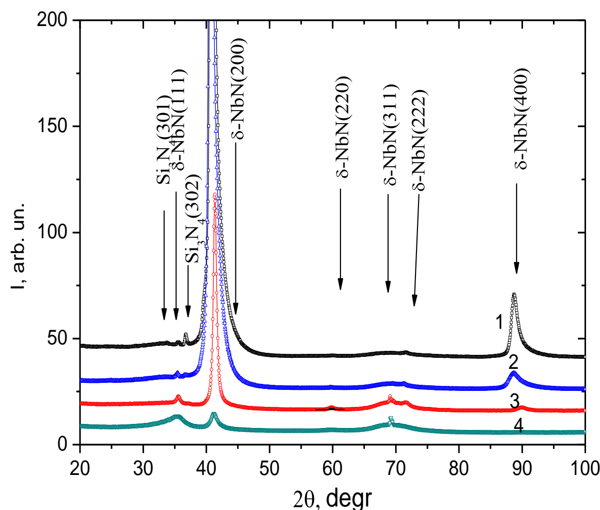

Fig. 3 – XRD spectra of Nb-Si-N films at 1. U_s = 0 V, 2. U_s = - 20 V, 3. U_s = - 40 V, 4.U_s= - 70 V

The results of the XPS examination of the as deposited and annealed NbN and Nb-Si-N films are presented in Fig. 4. It is known that a native oxide grows on Nb compounds when exposed to air [12], and the peaks at 204.07 eV and 206.88 eV can be assigned to Nb 3d in NbN (203.97 eV [13]) and $Nb_2N_{2-x}O_{3+x}$ (207.0 eV [14]). For NbN films, the peak at 397.4 eV in the N 1s spectrum is determined by Nb-N bonds, whereas for Nb-Si-N films, this peak is located around 397.2 eV, and can be assigned to N 1s in NbN (397.4 eV [12]).

We suppose that the asymmetry of the N 1s peak can be caused by the Si-N bonds in Si_3N_4 (397.8 eV [14]). XPS measurements of the Si 2p spectrum provide further information on the Si bonding in the Nb-Si-N films (cf. Fig. 4). The peak at a binding energy of 101.7 eV is assigned to Si in Si_3N_4 (101.7 eV [14]), and a shoulder at 103.3 eV in the Si 2p spectrum of the annealed films is supposed to be due to the Si-O bonds in SiO_2 (103.5 eV [14]). Finally, the O 1s spectra of the NbN and Nb-Si-N films are centered around 530.5 eV and 530.9 eV, respectively, and can be attributed to the Nb-O bonds in Nb_2O_5 (530.4 eV) and Nb_2O_2 (530.7 eV [14]), respectively. In the case of Nb-Si-N films, the Si-

O bonds in SiO_2 can form the wide tail around 532.9 eV [14] (cf. Fig. 4). Using the XPS data (cf. Fig. 4), we estimated the niobium, nitrogen and silicon contents (C_{Nb}, C_N and C_{Si}, respectively) in NbN and Nb-Si-N films. It was found that C_{Nb} = 44.5 at.%, C_N = 55.5 at.% for NbN films and and C_{Nb} = 45.1 at.%, C_N = 43.2 at.% and C_{Si} = 1.7 at.% for Nb-Si-N films.

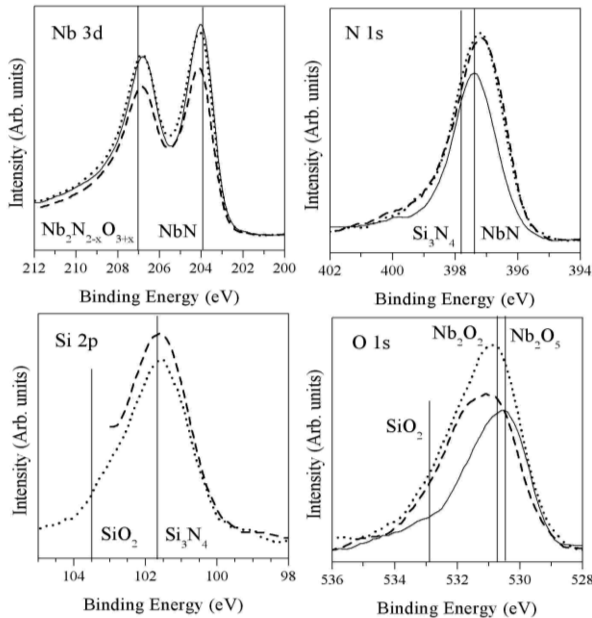

Fig. 4 – XPS spectra of the core levels in NbN (solid line), Nb-Si-N (dashed line) and annealed at 1000°C Nb-Si-N (dotted line) films deposited at P_w=14.3 W/cm^2. The vertical lines denote the binding energies of the XPS peaks of: Nb 3d in NbN, 203.97 eV [13] and $Nb_2N_{2-x}O_{3+x}$, 207.0 eV [14]; N 1s in NbN, 397.4 eV [12] and Si_3N_4, 397.8 eV [14]; Si 2p in Si_3N_4, 101.7 eV and SiO_2, 103.5 eV [14]; O 1s in Nb_2O_5, 530.4 eV, Nb_2O_2, 530.7 eV and SiO_2, 532.9 [14]

Comparison of the results presented in Fig. 1-4 enables us to establish the structure of the NbN and Nb-Si-N films. The NbN films are nanostructured, and the Nb-Si-N films have a nanocomposite structure, and represent an aggregation of δ-NbN_x nanocrystallites embedded into the amorphous Si_3N_4 tissue (nc-δ-NbNx/a-Si_3N_4). In contrast to NbN films, Nb-Si-N films are textured with the preferable (200) grain orientation. The films contain oxygen in the view of niobium oxides. For Nb-Si-N films, we also suppose that, oxygen forms SiO_2 that is segregated along grain boundaries. We note that, despite the larger grain sizes, the surface roughness of the Nb-Si-N films is smaller as compared to that of the NbN films. One can assume that the amorphous SiN_4 tissue in nanocomposite Nb-Si-N films smears the relief of the film surface, for this reason, the surface roughness of the nanocomposite films should be lower than that of NbN films.

The dependence of nanohardness (H) and elastic modulus (E) on indenter penetration (L) of the deposited films are presented in Fig. 5 and Fig. 6. It is seen that, beginning with 75 nm, the nanohardness practically does not depend on L. The elastic modulus decreases upon a reaching maximum values at L = 50 nm. These results point out that the soft silicon substrate does not exert influence on the nanohardness of the films. The elastic modulus of the films turns out to be more sensitive to the substrates, especially at high L.

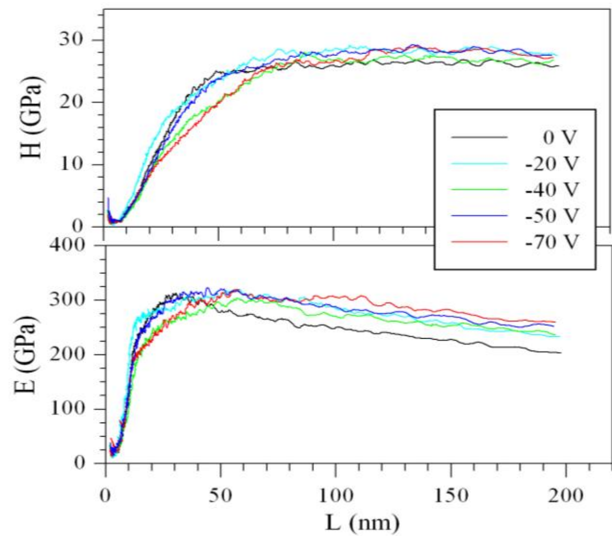

Fig. 5 – Dependences of the nanohardness (H) and elastic modulus (E) on nanoindenter penetration (L) for the NbN films deposited at various bias voltage

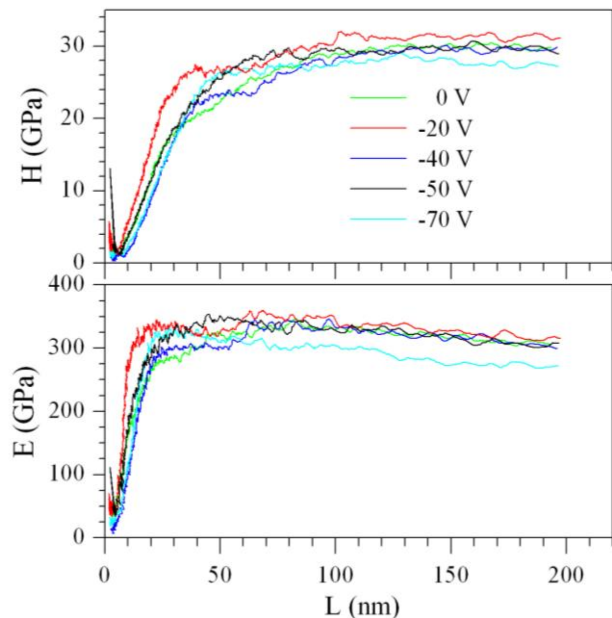

Fig. 6 – Dependences of the nanohardness (H) and elastic modulus (E) on nanoindenter penetration (L) for the Nb−Si−N films deposited at various bias voltage

4. CONCLUSIONS

The NiCoCrAlY coating on the flat specimens of nickel base superalloy JS6U were produced by a multi-chamber detonation sprayer. The MCDS application allows to form a dense hard layer with porosity below 1 %. Results of this work open up new prospects for further elaboration of new technologies to making protective NiCoCrAlY coatings which can enhance properties of nickel base superalloy.

REFERENCES

1. A.D. Pogrebnjak, A.G. Ponomarev, A.P. Shpak, *Phys. Usp.* **55**, 270 (2012).
2. A.D. Pogrebnjak, V.M. Beresnev, *Nanocoatings, Nanosystems, Nanotechnologies* (Bentham Sci. Pub.: Sharjah: 2012).
3. A.D. Pogrebnjak, V.M. Beresnev, A.A. Demianenko, *Phys. Solid State* **54**, 1882 (2012).
4. R. Krause-Rehberg, A.D. Pogrebnyak, O.V. Sobol', *Phys. Metals and Metallogr.* **114** No8, 672 (2013).
5. A.D. Pogrebnjak, Yu.A. Kravchenko, S.B. Kislitsyn, *Surf. Coat. Tech.* **201** No6, 2621 (2006).
6. A.D. Pogrebnjak, S. Bratushka, V.I. Boyko, *Nucl. Instr. & Meth.* **145** No3, 373 (1998).
7. A.D. Pogrebnjak, A.D. Mikhaliov, N.A. Pogrebnjak, *Phys. Lett.* **241**, 357 (1998).
8. V.N. Zhytomirsky, *Surf. Coat. Technol.* **201**, 6122 (2007).
9. G.A. Fontalvo, V. Terziyska, C. Mitterer, *Surf. Coat. Technol.* **202**, 1017 (2007).
10. N. Hayashi, I.H. Murzin, I. Sakamoto, M. Ohkubo *Thin Solid Films* **259**, 146 (1995).
11. G. Cappuccio, U. Gambardella, A. Morone, S. Orlando, G.P. Patisi, *Appl. Surf. Sci.* **109**, 399 (1997).
12. J. Wang, Z. Song, K. Xu, *Surf. Coat. Technol.* **201**, 4931 (2007).
13. J.J. Jeong, C.M. Lee, *Appl. Surf. Sci.* **214**, 11 (2003).
14. G. Beamson, D. Briggs, *High Resolution XPS of Organic Polymers, The Scienta ESCA300 Database* (Wiley Interscience: 1992).